Electrically tunable chiral liquid crystal lens arrays

Kelum Perera[1,2], Nilanthi Haputhantrige[1,2], Md Sakhawat Hossain,[2,3]
Md Mostafa[2,3], Alex Adaka[2,3], Oleg D. Lavrentovich[1,2,3], and Antal Jákli[1,2,3]
[1]Department of Physics, Kent State University, Kent OH, 44242, USA
[2]Advanced Materials and Liquid Crystal Institute, Kent State University, Kent OH, 44242, USA
[3]Materials Science Graduate Program, Kent State University, Kent OH, 44242, USA

Abstract

Lenses with tunable focal lengths play important roles in nature as well as modern technologies. In recent years, the demand for electrically tunable lenses and lens arrays has grown, driven by the increasing interest in augmented and virtual reality, as well as sensing applications. In this paper, we present a novel type of electrically tunable microlens utilizing polymer-stabilized chiral ferroelectric nematic liquid crystal. The lens offers a fast response time (5ms) and the focal length can be tuned by applying an in-plane electric field. The electrically induced change in the lens shape, facilitated by the remarkable sensitivity of the chiral ferroelectric nematic to electric fields, enables the tunable focal length capability. The achieved performance of this lens represents a significant advancement compared to electrowetting-based liquid lenses and opens exciting prospects in various fields, including biomimetic optics, security printing, solar energy concentration, and AR/VR devices.

I. Introduction

Microlens arrays based on liquid crystals (LC-MLAs) have found diverse applications in technologies such as optic fiber switches[1,2], display systems[3,4], holographic imaging[5,6], and more. In recent years, several fabrication methods have been explored for manufacturing microlens arrays, including hole-patterned electrodes[7,8], inkjet printing[9], photoalignment[10], optically hidden dielectric structures[11,12], and polymer stabilized liquid crystal systems [13–15]. LC lenses with tunable properties can be achieved through various methods[16–22]. The GRIN (Gradient Refractive Index) LC lens utilizes a specific electrode arrangement to create a non-uniform electric field within the LC medium[23]. This non-uniform electric field induces a polarization-dependent spatial profile of

the refractive index. As a result, GRIN LC lenses offer electrically controlled focal length tunability and adaptability.

The LC lenses designed with fixed curved shapes, incorporate an electric field that induces director realignment, leading to a change in the effective refractive index[24]. However, unlike other tunable LC lenses, the electric field does not alter the curved shape of these lenses. On the other hand, electric tuning of the lens shape is the defining feature of the isotropic liquid lenses controlled by the phenomenon of electrowetting.

Recently, we have introduced an electrically tunable LC lens with distinct advantages over electrowetting lenses, such as our LC lens exhibits faster tuning capabilities and operates at lower voltages[25] using a room temperature ferroelectric nematic liquid crystal mixture FNLC 919 from Merck. Here we present the results on another room temperature ferroelectric nematic liquid crystals, FNLC1571. We find very similar behavior with slightly faster switching time and larger focal distance tunability in a wider applied field range. These results show that this novel polarization independent tuning of the focal length of ferroelectric nematic liquid crystal containing microlenses have potential for further improvements.

II. Materials and Methods

The precursor comprises of 60 wt.% ferroelectric nematic LC host abbreviated FNLC 1571 and synthesized by Merck, (clearing point Tc = 88.0°C), 17wt.% nematic liquid crystal 5CB, 7 wt.% chiral dopant BDH1281 (HTP~100 μm^{-1}), 15 wt.% photocurable monomers (5wt.% TMPTA, 5wt.% RM 257, and 5wt.% EHA, see Figure 1(a) for the chemical structures) and 1 wt.% photoinitiator, Irgacure 651. FNLC 1571 has two nematic phases N_1 and N_2 above the N_F phase. The phase sequence in cooling is I 88°C N_1 62°C N_2 48°C N_F 8°C Cr. The monomer ratios were carefully adjusted to balance the operation voltage and response time. BDH1281 is employed due to its high helical twisting power. To test the electro-optical properties, the precursor was heated to 90°C, stirred using a magnetic stirrer and then capillary filled into an in-plane switching (IPS) cell. The 9.8 μm thick IPS cell consisted of interdigitated electrodes on the bottom substrate (IPS 15/15- electrode width w = 15μm, spacing between electrode l = 15μm). The cell was photopolymerized for 30 min at room temperature using UV light (Black-Ray, Model B-100AP/R intensity ~ 75 mW/cm^2) to achieve an optically isotropic polymer stabilized material.

To fabricate the lens, we spin-coated 10 nm thick layer of UV curable adhesive Norland (NOA) on IPS10/10 substrates and UV cured it for 30 min. Nickel Ted Pella TEM grids were cleaned in methanol with an ultrasonic cleaner (Branson B200) before use. Each cell in the double mesh is 20 μm thick and has a side length of a = 100 μm. The grid arrays were glued to NOA-coated glass substrates by applying a thin layer of adhesive on the bottom of the grid cell walls and placing the grid carefully on top of the glass, avoiding any spreading of the glue on the glass and the glue was cured using 365 nm UV light (Black-Ray, Model B-100AP/R) for 10 minutes to permanently settle the grids on top of the NOA coated glass. About 1 μL of LC mixture was put on top of the grid using a micropipette and compressed air with a pressure of 2 kPa was applied to the grid for $2s$ at ~45° to push a fraction of the LC out from the cells to make an underfilled state to form the Plano-concave microlenses. Then the sample was partially photopolymerized at room temperature in open air for 5 min using a 365 nm wavelength f $5mW/cm^2$ intensity UV light source. The top protective cover glass was assembled with ~20 μm spacers to protect the lens array from dust.

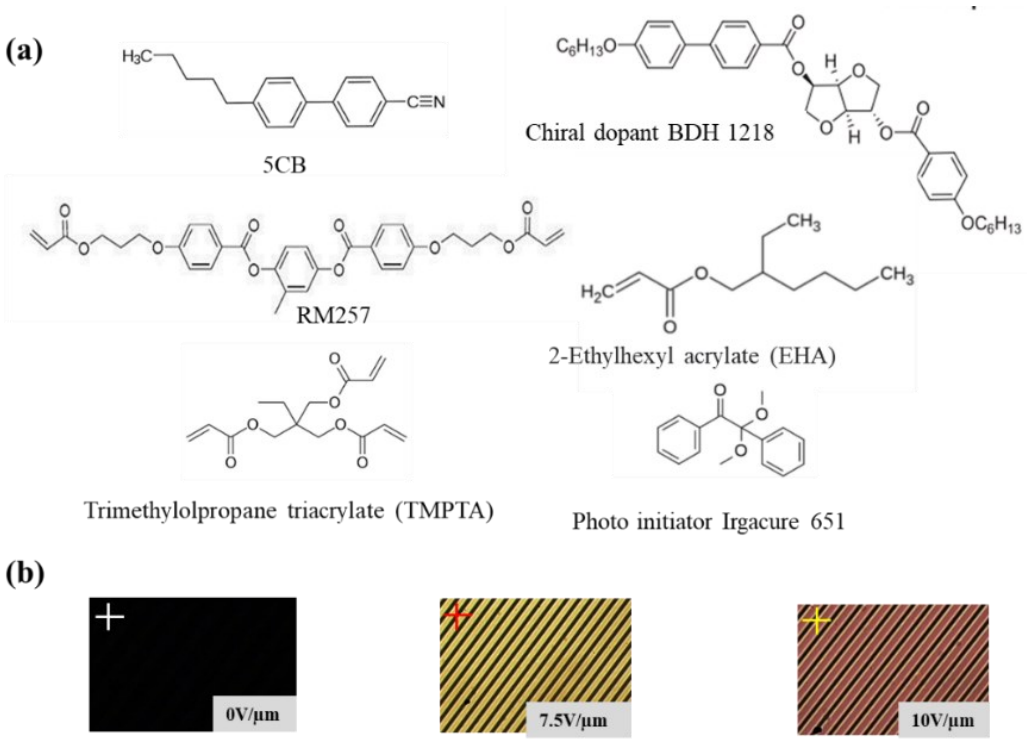

Figure 1: (a) Chemical structure of the materials used to engineer polymer stabilizes ferroelectric nematic mixture. (b): Polarized Optical Microscopy (POM) images of a 9.8 μm thick IPS *cell under crossed polarizers with different applied electric fields.*

II. Results

The polymer-stabilized LC mixture is optically isotropic, i.e., dark under crossed polarizers as shown in ***Figure 1 (b).*** When applying an electric field, the picture brightens due to the in-plane field-induced birefringence $\delta n(V)$. The film shows low saturation voltage (~5.5V/μm) in IPS mode, large electric field induced birefringence ~0.08 @ 10V/μm for 550nm green light. The haze of the films was measured using an integrated sphere of a UV-3600 Plus Shimadzu UV-Vis-NIR Spectrophotometer and shows minimal haze <1% at 550nm. We measured the response time of the film using 1kHz square pulse with 60Vpp. The rise (decay) time is usually defined as the time taken for switching between 10% and 90% (90% and 10%) of the maximum transmittance was 300 μs and the falling time was 240μs.

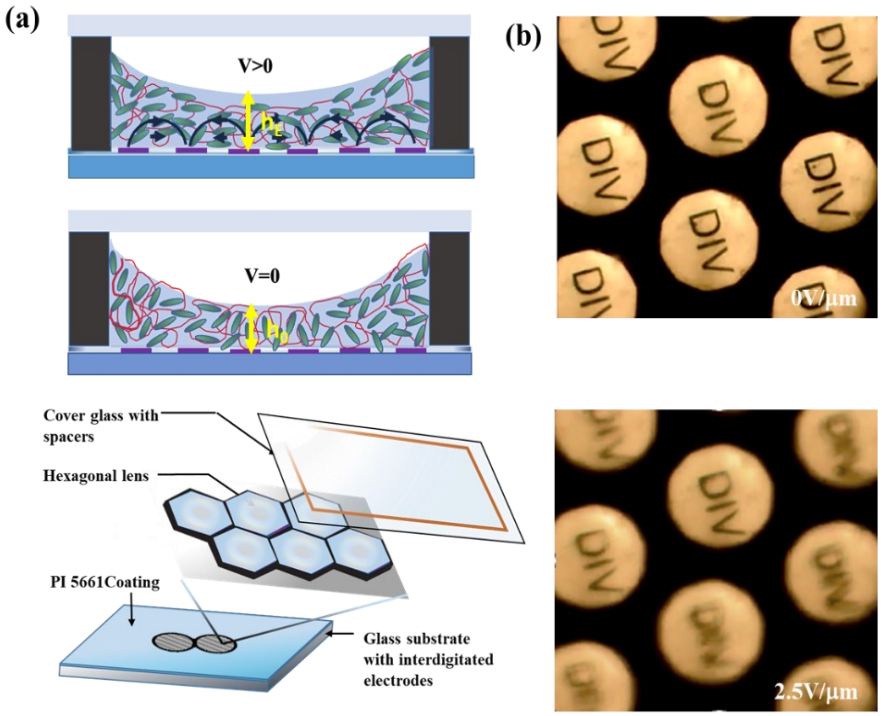

Figure 2(a): Schematic of the fabricated lens and sketch of the side-view of a single grid with interdigitated electrodes and the Plano-concave lens of the polymer-stabilized liquid crystal covered with a glass slide before and after applying field indicating changes in the height in the center due to electric filed induced shape changed. (b)The top-right picture shows a focused array of the images of letters "DIV" at 0 V/μm field and bottom-right picture shows how these images become defocused when 2.5Vpp/μm 1 kHz field is applied between the interdigitated electrodes.

The Schematics of the fabricated lens and the optical imaging properties of the plano-concave lenses are illustrated in **Figure 2(b).** The top-right picture shows the focused images of the object (letters DIV) created by the microlenses at zero electric field. Multiple images of the object were get defocused after applying an electric field between the interdigitated electrodes as shown in the bottom-right picture in ***Figure 2(b)***.

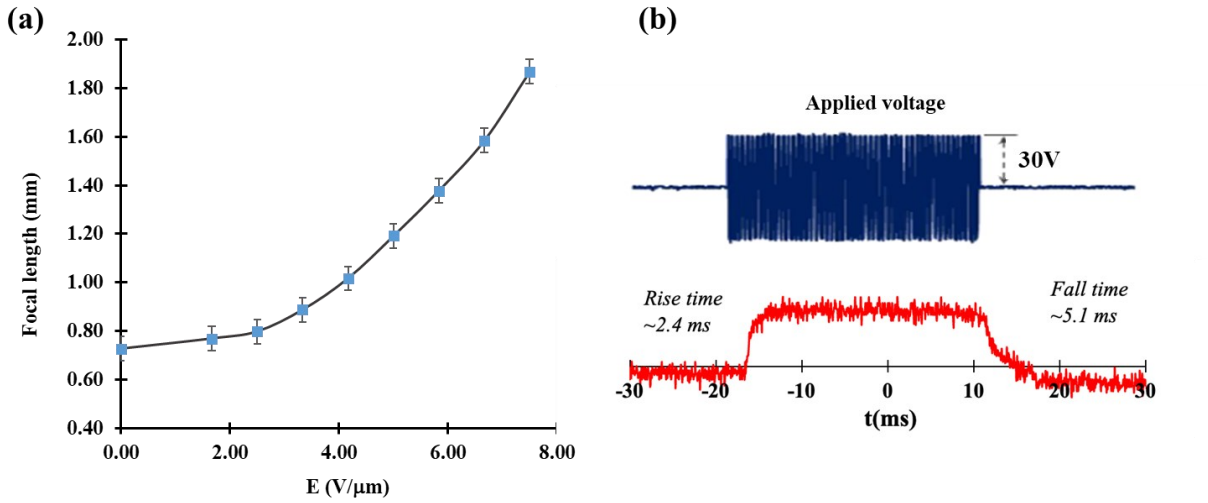

Figure 3: Focal length as a function of electric field and the response time of the microlens array. (a) Electric field dependence of the absolute value of focal length measured experimentally. (b) The time dependence of the defocusing and refocusing due to 1 kHz, 60Vpp square wave field pulse.

Figure 3(a) shows the electric field dependence of the focal length determined from the lens equation $f = \frac{d_o \times d_i}{d_i - d_o}$, where d_o and d_i are the measured object and virtual image distances. The fabricated microlenses have a focal length $-0.73\ mm$ before applying the field. The focal length can be tuned to $-1.9\ mm$ at $7.5 V/\mu m$. **Figure 3(b)** shows the response of the lens to 1 kHz, $60 V_{pp}$ square wave pulse (defocusing) takes 2.4 ms , while the refocusing (relaxation back to the original shape) happens in $5ms$.

Figure 4 shows that the height of the lens measured from the bottom as a function of the distance from the center of the hexagonal opening. The LC-air interface profile is measured using a digital holographic microscope (DHM). The curvature is decreasing with increasing in-plane electric field in the $0 - 2.7\ V/\mu m$ field range. The lower inset shows the 3D rendering of the side view of the lens while the upper inset with color coding shows the top view at $2V/\mu m$ in-plane

field. One can see that the lens profile is axially symmetric and not biased by the electric field, i.e., the cross sections are the same when taken along different directions.

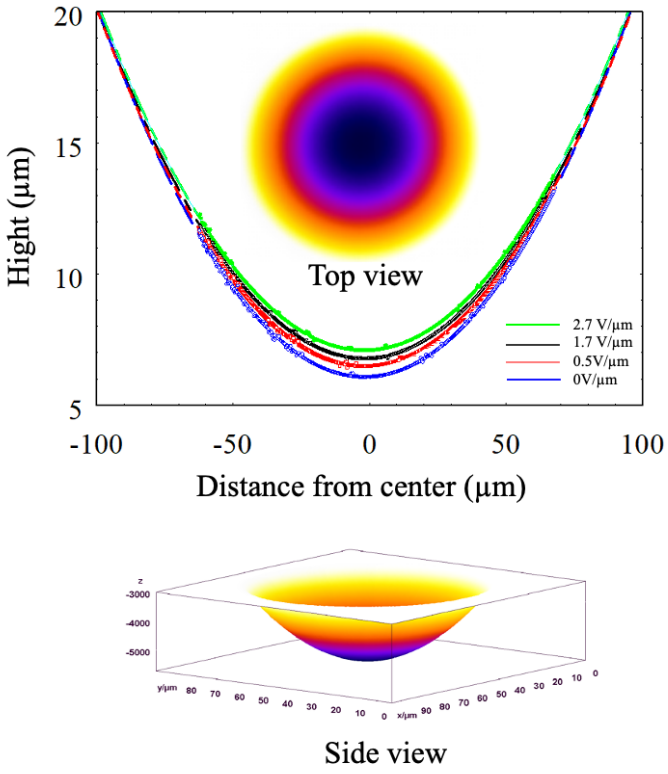

Figure 4 Height profile of the lens measured from the bottom as a function of the distance from the center of the lens. The height profile data were obtained with a Digital Holographic Microscope (DHM); dotted lines are the best fits using quadratic function. The top inset shows the 3D rendering of the shape and shows that the lens shape remains axially symmetric when acted upon by a 2V/μm in-plane field. The bottom image shows the side view of the recreated using DHM data.

III. Discussion

The electric field dependence of the focal length $f(E)$ of a parabolic-shaped microlens can be expressed as[16] $f(E) \approx \frac{a^2}{2(n(E)-1)\cdot(h_c(E)-h_b(E))}$. In this equation $h_b(E)$ and $h_c(E)$ are the field dependent thickness at the grid boundary (aperture) and at the center, respectively. The field-dependent refractive index $n(E)$ can be written as $n(E)=n_i+\delta n(E)$, where $n_i = \frac{n_\parallel+2n_\perp}{3}$ is the refractive index in the optically isotropic state at zero field applied; $n_\parallel$ and $n_\perp$ are the refractive indices of the liquid crystal along and perpendicular to the director, respectively. Taking $n_\perp \approx$

1.53 and $n_{\parallel} = 1.75$ for FNLC 919 [26], we get $n_i \approx 1.60$. With this, from the measured $f(E)$ (see Figure 3a), we get $n(E)$~1.61, i.e., $\delta n = 0.01$ at $2.7V/\mu m$.

IV. Summary

In this paper we have demonstrated an array of electrically tunable polymer stabilized chiral ferroelectric nematic liquid crystal microlenses. The focal length of the microlenses can be tuned with a few $V/\mu m$ in-plane electric fields within about 5 ms. This remarkable performance was achieved by the field-induced shape variation of the lens, which is a result of the electric field-induced stresses in the polymer-stabilized chiral ferroelectric nematic. These results represent a significant leap compared to the electrowetting-induced tuning of liquid lenses and open new realms in various applications such as biomimetic optics, security printing, solar concentration, and AR/VR devices.

VI. Acknowledgement

This work was supported by NSF grants DMR-2210083 (AJ) and ECCS-2122399 (ODL). The material FNLC 1571 was provided by Merck Electronics KGsA, Darmstadt, Germany.

VII. References

1. Duparre, J., Radtke, D. & Dannberg, P. Implementation of field lens arrays in beam-deflecting microlens array telescopes. *Appl Opt* **43**, (2004).
2. Noponen, E., Turunen, J. & Vasara, A. Electromagnetic theory and design of diffractive-lens arrays. *Journal of the Optical Society of America A* **10**, 434 (1993).
3. Xiong, Z., Wang, Q., Li, S., Deng, H. & Ji, C. Partially-overlapped viewing zone based integral imaging system with super wide viewing angle. *Opt Express* **22**, 22268 (2014).
4. Luo, L. *et al.* 360-degree viewable tabletop 3D display system based on integral imaging by using perspective-oriented layer. *Opt Commun* **438**, 54–60 (2019).
5. Velez, A., Barrera-ramírez, J. F. & Torroba, R. Optics & Laser Technology One-step reconstruction of assembled 3D holographic scenes. *Opt Laser Technol* **75**, 146–150 (2015).
6. Pang, X., Jiang, S. & Dong, J. Dynamic holographic imaging of real-life scene. *Opt Laser Technol* **119**, 105590 (2019).

7. Huang, Y., Chen, C. & Shen, T. 25 . 1 Invited Paper : High Resolution Autostereoscopic 3D Display with Scanning Multi-Electrode Driving Liquid Crystal (MeD-LC) Lens. **3**, 336–339 (2009).
8. Algorri, J. F. *et al.* Tunable liquid crystal multifocal microlens array. *Sci Rep* **7**, 17318 (2017).
9. Kamal, W. *et al.* Electrically Tunable Printed Bifocal Liquid Crystal Microlens Arrays. **2000578**, (2020).
10. Wu, J. *et al.* Electrically Tunable Microlens Array Enabled by Polymer-Stabilized Smectic Hierarchical Architectures. **2201015**, 1–7 (2022).
11. Cui, J., Fan, H. & Wang, Q. A polarisation-independent blue-phase liquid crystal microlens using an optically hidden dielectric structure. *Liq Cryst* **44**, 643–647 (2017).
12. Asatryan, K., Presnyakov, V., Tork, A., Zohrabyan, A. & Galstian, T. Optical lens with electrically variable focus using an optically hidden dielectric structure. **18**, 3420–3425 (2010).
13. Li, R. *et al.* A blue-phase liquid crystal lens array based on dual square ring-patterned electrodes. *Liq Cryst* **46**, 1266–1272 (2019).
14. Chu, F. *et al.* A polarisation-independent blue-phase liquid crystal lens array using gradient electrodes. *Liq Cryst* **45**, 715–720 (2018).
15. Li, Y. *et al.* Polymer-Stabilized Blue Phase Liquid Crystals for Photonic Applications. *Adv Mater Technol* **1**, 1600102 (2016).
16. Perera, K., Padmini, H. N., Mann, E. & Jákli, A. Polymer Stabilized Paraboloid Liquid Crystal Microlenses with Integrated Pancharatnam–Berry Phase. *Adv Opt Mater* **10**, 1–8 (2022).
17. Perera, K., Nemati, A., Mann, E. K., Hegmann, T. & Jákli, A. Converging Microlens Array Using Nematic Liquid Crystals Doped with Chiral Nanoparticles. *ACS Appl Mater Interfaces* **13**, 4574–4582 (2021).
18. Perera, K., Nemati, A., Mann, E., Hegmann, T. & Jákli, A. I. Optical properties of nematic microlenses doped with chiral nanoparticles. in *Liquid Crystals XXIV* (ed. Khoo, I. C.) 114720O (2–7) (SPIE, 2020). doi:10.1117/12.2568570.
19. Cheng, C., Chang, C. A., Liu, C. & Yeh, J. A. A tunable liquid-crystal microlens with hybrid alignment. **365**,.

20. In, Z. H. X. *et al.* Graphene-based adaptive liquid-crystal microlens array for a wide infrared spectral region. **9**, 183–194 (2019).
21. Popov, P., Honaker, L. W., Mirheydari, M., Mann, E. K. & Jákli, A. Chiral nematic liquid crystal microlenses /639/301 /639/624 /123 /132/124 /128 /129 article. *Sci Rep* **7**, 1–9 (2017).
22. Xiong, B. G. *et al.* Phototunable Microlens Array Based on Polymer Dispersed Liquid Crystals. 1082–1086 (2009) doi:10.1002/adfm.200801335.
23. Kwon, H., Kizu, Y., Kizaki, Y., Ito, M. & Kobayashi, M. A Gradient Index Liquid Crystal Microlens Array for Light-Field Camera Applications. **27**, 836–839 (2015).
24. Bailey, J., Morgan, P. B., Gleeson, H. F. & Jones, J. C. Switchable liquid crystal contact lenses for the correction of presbyopia. *Crystals* vol. 8 Preprint at https://doi.org/10.3390/cryst8010029 (2018).
25. Perera, K. *et al.* Electrically Tunable Polymer Stabilized Chiral Ferroelectric Nematic Liquid Crystal Microlenses. *Advanced Materials* under review (2023).
26. Yu, J.-S., Lee, J. H., Lee, J.-Y. & Kim, J.-H. Alignment properties of a ferroelectric nematic liquid crystal on the rubbed substrates. *Soft Matter* 2446 (2023) doi:10.1039/d3sm00123g.